

## A comparative molecular dynamics study of diffusion of *n*-decane and 3-methyl pentane in Y zeolite<sup>†</sup>

F G PAZZONA<sup>1,\*</sup>, B J BORAH<sup>1</sup>, P DEMONTIS<sup>3</sup>, G B SUFFRITTI<sup>3</sup> and S YASHONATH<sup>1,2</sup>

<sup>1</sup>Solid State and Structural Chemistry Unit,

<sup>2</sup>Center for Condensed Matter Theory, Indian Institute of Science, Bangalore 560 012

<sup>3</sup>Dipartimento di Chimica, Università di Sassari, Via Vienna 2 I-07100 Sassari, Italy

e-mail: fpazzona@uniss.it; yashonath@sscu.iisc.ernet.in

**Abstract.** Molecular dynamics simulations are reported on the structure and dynamics of *n*-decane and 3-methylpentane in zeolite NaY. We have calculated several properties such as the center of mass-center of mass rdf, the end-end distance distribution, bond angle distribution and dihedral angle distribution. We have also analysed trajectory to obtain diffusivity and velocity autocorrelation function (VACF). Surprisingly, the diffusivity of 3-methylpentane which is having larger cross-section perpendicular to the long molecular axis is higher than *n*-decane at 300 K. Activation energies have been obtained from simulations performed at 200 K, 300 K, 350 K, 400 K and 450 K in the NVE ensemble. These results can be understood in terms of the previously known levitation effect. Arrhenius plot has higher value of slope for *n*-decane (5.9 kJ/mol) than 3-methylpentane (3.7 kJ/mol) in agreement with the prediction of levitation effect.

**Keywords.** Hydrocarbon; diffusion; levitation effect; zeolite; separation.

### 1. Introduction

Linear and branched hydrocarbons exist in the crude oil or even in the output of the refineries which separate large hydrocarbons from smaller hydrocarbons.<sup>1–12</sup> Frequently, linear hydrocarbons need to be separated from the branched hydrocarbons before required conversion can be carried out to obtain industrially essential chemicals. For this reason, separation of branched from linear hydrocarbons is of considerable interest.

From the point of view of a fundamental understanding also, the motion of linear and branched hydrocarbons provided by two contrasting and quite different molecules. A linear molecule typically has larger number of torsional degrees of freedom than a branched hydrocarbon. Larger the branching, lower the number of torsional degrees of freedom. Here, we do not consider torsional degrees of freedom involving hydrogens. Thus, neopentane has no torsional degrees of freedom but isopentane has one torsional degree of freedom whereas *n*-pentane has two torsional degrees of freedom. Most hydrocar-

bons involve only one or more branches on the primary backbone. In addition, molecular cross-section perpendicular to the long molecular axis is larger, higher the branching. This cross-section provides an idea of the size of the molecule relevant to diffusion since this cross-section determines size of the bottleneck that is required for the molecule to diffuse through the pore network within a zeolite.

Previous studies have shown that the self diffusivity of the diffusant exhibits a maximum as a function of the size of the diffusant for guests in zeolites.<sup>13</sup> This has been investigated through molecular dynamics studies of monatomic sorbates in different zeolites. Such a maximum is seen to exist irrespective of the geometrical and topological details of the pore network. The origin of this maximum in self diffusivity can be traced to the mutual cancellation of force exerted on the diffusant or sorbate by the medium (zeolite).<sup>14–16</sup> Such a cancellation occurs when the diameter of the diffusant is comparable to the void diameter. If the void diameter is varying along the diffusion path then the narrowest part of the void diameter, the bottleneck diameter is to be considered. This is also related to changes in entropy after adsorption.<sup>17</sup>

Here we investigate diffusion of *n*-decane and 3-methylpentane in zeolite NaY. The reason for this

<sup>†</sup>Dedicated to the memory of the late Professor S K Rangarajan

\*For correspondence

study arises from the fact that branched hydrocarbons in general have a larger molecular cross-section perpendicular to their long molecular axis as compared to linear hydrocarbons. The dimensionless parameter known as the Levitation parameter  $\gamma$  is given by

$$\gamma = \frac{\sigma_{\perp}}{\sigma_n}, \quad (1)$$

where  $\sigma_{\perp}$  is the molecular cross-section perpendicular to the molecular axis and  $\sigma_n$  is the bottleneck diameter. The latter is a characteristic of the void network within the zeolite. Since molecular cross-section perpendicular to the molecular axis is large for branched alkanes as compared to linear hydrocarbons, they can be closer to the bottleneck diameter for certain choice of the zeolite. In fact, as we shall see, 3-methylpentane has a diameter significantly closer to the 12-ring window of zeolite NaY as compared to *n*-decane. In figure 1 we show a plot of self diffusivity against  $\gamma$  for spherical monatomic guests in zeolite NaY. The dependence against  $\gamma$  is universal except for minor details and does not depend on the nature of the guest.

The cross-section dimensions of *n*-decane are  $4.85 \times 4.15 \text{ \AA}$  while 3-methylpentane has  $6.22 \times 5.48 \text{ \AA}$ .<sup>18</sup> The larger of these dimensions,  $6.22 \text{ \AA}$ , is that of 3-methylpentane. The factor in the numerator of (1) given by  $2^{1/6} \times \sigma_{gh}$  (where  $\sigma_{gh}$  is the Lennard-Jones parameter for guest–host interaction) for 3-methylpentane is  $6.98 \text{ \AA}$  while it is  $5.44 \text{ \AA}$  for

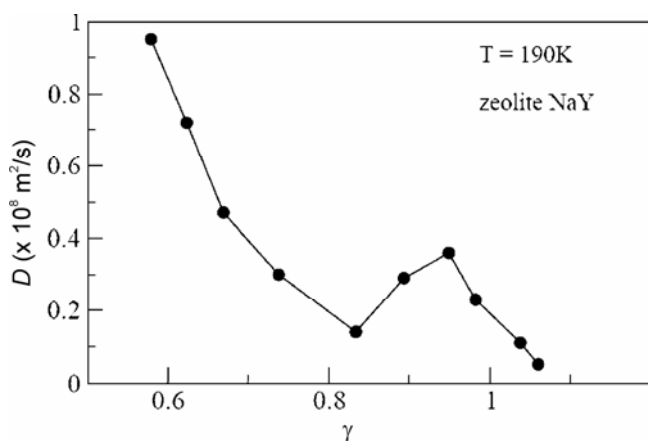


**Figure 1.** A plot of diffusion coefficient as a function of  $\gamma$  for NaY zeolite. Here linear regime extends up to the first minimum, anomalous regime is for the region beyond the minimum. Note that the peak is seen close to  $\gamma = 1$ .

*n*-decane. It is known that zeolite NaY has a window diameter of  $7.4 \text{ \AA}$ . Using this, the corresponding  $\gamma$  values for 3-methylpentane is 0.94 while that for *n*-decane is 0.73. From the plot of  $D - \gamma$  we see that 0.94 lies in the anomalous regime where the diffusivity exhibits a maximum whereas *n*-decane lies in linear regime which has much lower value for  $D$ . Zeolite has been modelled as a flexible framework with the help of the potential proposed by Demontis et al<sup>19</sup> *n*-decane has been modelled with all torsional degrees of freedom using united atom approach of Jorgensen.<sup>20</sup>

## 2. Intermolecular potential and molecular dynamics simulations

### 2.1 Hydrocarbon

The united atom approach is used in modelling the hydrocarbons.  $\text{CH}_3$ ,  $\text{CH}_2$  and  $\text{CH}$  are considered as single beads. The non-bonded interactions between two sites belonging to two different molecules or sites belonging to same molecule but separated by more than three bonds are modelled using Lennard–Jones (LJ) potential.

$$U(r_{ij}) = 4\varepsilon_{ij} \left[ \left( \frac{\sigma_{ij}}{r_{ij}} \right)^{12} - \left( \frac{\sigma_{ij}}{r_{ij}} \right)^6 \right], \quad (2)$$

where  $r_{ij}$ ,  $\varepsilon_{ij}$  and  $\sigma_{ij}$  are distance between two interaction sites, LJ is well depth and size of the interaction site respectively. The LJ parameters are listed in table 1.

**Table 1.** Lennard–Jones parameters of hydrocarbon–hydrocarbon interaction.<sup>21</sup>

Atom types	$\sigma$ (Å)	$\varepsilon/k_B$ (K)	Remarks
$\text{CH}_3\text{--CH}_3$	3.85	70.0	Methyl side chains
$\text{CH}_3\text{--CH}_3$	3.91	104.0	General
$\text{CH}_2\text{--CH}_2$	3.93	45.8	–
$\text{CH--CH}$	3.85	39.7	–

**Table 2.** Bond stretching and bond angle bending parameters for hydrocarbons.<sup>21</sup>

Bond stretching	$r_0$ (Å)	$k_r/k_B$ (K)
$\text{CH}_x\text{--CH}_y$	1.54	96500
Bond angle bending	$\theta_0$	$k_\theta/k_B$
$\text{CH}_x\text{--CH}_2\text{--CH}_y$	114.0	62500
$\text{CH}_x\text{--CH--CH}_y$	109.47	62500

**Table 3.** Torsional potential parameters for hydrocarbons.<sup>21</sup>

Dihedral angle	$V_0/k_B$ (K)	$V_1/k_B$ (K)	$V_2/k_B$ (K)	$V_3/k_B$ (K)
CH <sub>x</sub> -CH <sub>2</sub> -CH <sub>2</sub> -CH <sub>y</sub>	0	355.04	-68.19	791.32
CH <sub>x</sub> -CH <sub>2</sub> -CH-CH <sub>y</sub>	1416.3	398.3	139.12	-901.2
CH <sub>x</sub> -CH-CH-CH <sub>y</sub>	0	0	0	1635.7

**Table 4.** Bond stretching parameters for zeolite.

Bond	$r_0$ (Å)	$k_r/k_B$ (K)
Si-O	1.605	251383.2090

The cross interaction between two unlike sites is given by the Lorentz–Berthelot mixing rules.

$$\sigma_{ij} = \frac{1}{2}(\sigma_{ii} + \sigma_{jj}), \quad (3)$$

$$\varepsilon_{ij} = (\varepsilon_{ii}\varepsilon_{jj})^{1/2}. \quad (4)$$

The bond stretching and bond angle bending are modelled using harmonic potentials.

$$U(r) = \frac{k_r}{2}(r - r_0)^2, \quad (5)$$

$$U(\theta) = \frac{k_\theta}{2}(\theta - \theta_0)^2, \quad (6)$$

where  $r_0$  and  $\theta_0$  are the equilibrium bond length and bond angle respectively. The torsional motion is modelled using the following function

$$U(\phi) = V_0 + V_1(1 + \cos\phi) + V_2(1 - \cos 2\phi) + V_3(1 + \cos 3\phi). \quad (7)$$

The bond stretching and bond angle bending potential parameters are listed in table 2. The torsional potential parameters are given in table 3.

## 2.2 Zeolite

Flexible model of Demontis *et al*<sup>19</sup> is used to model the zeolite. A harmonic potential is used to model the Si–O bond stretching.

$$U(r) = \frac{k_r}{2}(r - r_0)^2, \quad (8)$$

where  $r_0$  is the equilibrium bond length. The bending of bond angle Si–O–Si and O–Si–O is modelled

using a function having higher order terms than the harmonic function.

$$U(\theta) = \frac{k}{2}(\theta - \theta_0)^2 + \frac{k'}{3}(\theta - \theta_0)^3 + \frac{k''}{4}(\theta - \theta_0)^4, \quad (9)$$

where  $\theta_0$  is the equilibrium bond angle. The bond stretching parameters are given in table 4 and the bond angle bending parameters are given in table 5.

The sodium are considered to be frozen throughout the simulation. They are not included in molecular dynamics integration. The LJ parameters of zeolite atoms are described in the table 6. The cross interaction parameters between zeolite atoms and hydrocarbon interaction sites are obtained by using the Lorentz–Berthelot mixing rule as explained above.

## 3. Simulation details

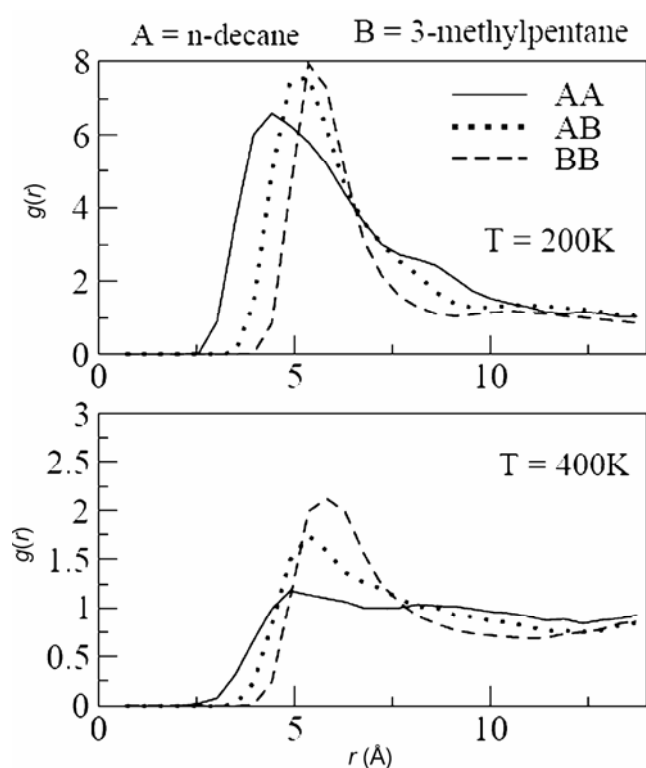
$3 \times 3 \times 3$  unit cells of zeolite NaY have been used in the simulation. The resulting simulation cell is of length 74.5608 Å. *n*-decane and 3-methylpentane were distributed uniformly in the cages of the zeolite. There are 36 *n*-decane and 36 3-methylpentane molecules or in all 72 distributed over 216  $\alpha$ -cages leading to a loading of 0.33 molecules per cage. All the simulations were performed in NVE ensemble using DLPOLY package.<sup>23</sup> A time-step of 1 fs has been found to yield good energy conservation. The velocity Verlet algorithm was used to solve the Newton's equations. Periodic boundary conditions were applied in all the three directions. A spherical cut-off of 14 Å was used. Initially a run of 500 ps was made during which the velocities were scaled to the desired temperature. A further run of 2 ns was made during which the position coordinates and velocities of the atoms were stored every 0.5 ps.

**Table 5.** Bond angle bending parameters for zeolite.

Bond angle	$\theta_0$	$k/k_B$ (K)	$k'/k_B$ (K)	$k''/k_B$ (K)
O–Si–O	109.2801	44650.685	–46993.6733	5018.126

**Table 6.** Lennard–Jones parameters for zeolite atoms (from Fuchs *et al*<sup>22</sup>).

Atom-type	$\sigma$ (Å)	$\epsilon/k_B$ (K)
Na–Na	2.584	50.34
O–O	3.0	93.53

**Figure 2.** Radial distribution functions of *n*-decane and 3-methylpentane. The upper graph is at temperature  $T = 200$  K and the lower one is at  $T = 400$  K. The solid line is for *n*-decane–*n*-decane, dashed line is for 3-methylpentane–3-methylpentane, and dotted line is for *n*-decane–3-methylpentane.

## 4. Results and discussion

### 4.1 Structure

Figure 2 shows centre of mass–centre of mass hydrocarbon–hydrocarbon rdf's at 200 K and 400 K for a 1 : 1 mixture of *n*-decane and 3-methylpentane in zeolite NaY. The peaks in the centre of mass(com)-

centre of mass(com) rdf show that two molecules of *n*-decane can approach each other more closely than either two molecules of 3-methylpentane or a molecule of 3-methylpentane and a molecule of *n*-decane. Further, a prominent shoulder is seen around 8 Å for *n*-decane. A somewhat less prominent shoulder is seen for *n*-decane–3-methylpentane com-com rdf. Since these molecules are large in size no second peak is observed before 14 Å.

With increase in temperature from 200 K to 400 K, significant changes are seen in all the rdf's. For *n*-decane–*n*-decane, the intensity of the rdf near 4 Å decreases significantly from around 6.5 at 200 K to 1 at 400 K. This clearly shows that by 400 K the hydrocarbon–hydrocarbon correlations for *n*-decane–*n*-decane essentially disappears. Correlation between 3-methylpentane–*n*-decane as well as 3-methylpentane–3-methylpentane is weaker at 400 K but persists. This change can be understood in terms of dimer interaction energies. Dimer interaction energy for 3-methylpentane–3-methylpentane is significantly stronger than 3-methylpentane–*n*-decane since a large number of methyl or methylene group of one molecule of 3-methylpentane can remain at close to optimum distances of methyl and methylene group of neighbouring molecule of 3-methylpentane. Optimum distance here is given by  $2^{1/6}\sigma$ , where  $\sigma$  is the Lennard–Jones parameter between the two interaction united atoms.

Figure 3 shows the end–end distance distribution, bond angle distribution and dihedral angle distribution. For *n*-decane,  $r(C_1 - C_6)$  as well as  $r(C_1 - C_{10})$  exhibits bimodal distributions. Such distribution indicates the availability of multiple dihedral angles and presence of multiple conformations for the long chain molecule. This leads to increase in flexibility with multiple energy minima for more than one combination of dihedral angle distribution. Thus for *n*-decane there are seven dihedral angles. In the configuration space consisting of  $E = E(\phi_1, \phi_2, \dots, \phi_7)$ , there are multiple minima of different energies. Thus for *n*-decane both  $r(C_1 - C_6)$  and  $r(C_1 - C_{10})$  shows that there are two minima one deeper than the other. The deeper minimum leads to more pronounced maxima in the probability distribution of

end–end distance. The peak near 6 Å for  $r(C_1 - C_6)$  corresponds to such a deeper minimum. In contrast, for 3-methylpentane, a unimodal distribution is seen for  $r(C_1 - C_4)$  since there is no flexibility. For  $r(C_1 - C_6)$ , availability of limited flexibility leads to the 3.8 Å shoulder.

The bond angle distribution of *n*-decane has a maximum around 114.0° and the distribution of 3-methylpentane has maximum around 110.0°. The distribution of 3-methylpentane is broader than that of *n*-decane. This is because of the structure of 3-methylpentane. It has three tetrahedral angles out of five bond angles. The dihedral angle distribution of *n*-decane has two peaks one at  $\phi = 60^\circ$  and the other at  $\phi = 180^\circ$  which corresponds to *gauche* and *trans* conformations respectively. The dihedral angle distribution of 3-methylpentane has two peaks corresponding to two dihedral angles around neighbouring bonds, viz.  $C_1 - C_3$  and  $C_3 - C_4$ .

## 4.2 Dynamics

Mean square displacements (MSD) of *n*-decane and 3-methylpentane are shown in figure 4 at a temperature of 300 K. The MSD's are linear with respect to time suggesting good statistics. The slope of these MSD's are computed by fitting a straight line to the MD data. Diffusivities are then computed from these slopes using Einstein's equation. The diffusivity of 3-methylpentane is  $4.35 \times 10^{-9} \text{ m}^2/\text{s}$  and that of

*n*-decane is  $3.18 \times 10^{-9} \text{ m}^2/\text{s}$ . The trend seen here is counter to what one expects from the kinetic theory. Since 3-methylpentane has larger cross-section we expect it to encounter frequent collisions leading to a slowing down of its motion. But here we see that it has higher diffusivity than *n*-decane. Thus, the higher self diffusivity of 3-methylpentane is possibly due to the levitation effect (LE). This is because of the larger cross-sectional dimension of 3-methylpentane which is comparable to the size of the window ( $\gamma = 0.94$ ) and hence falls in the anomalous regime of LE.

In figure 5, velocity autocorrelation functions (VACF) of *n*-decane and 3-methylpentane are

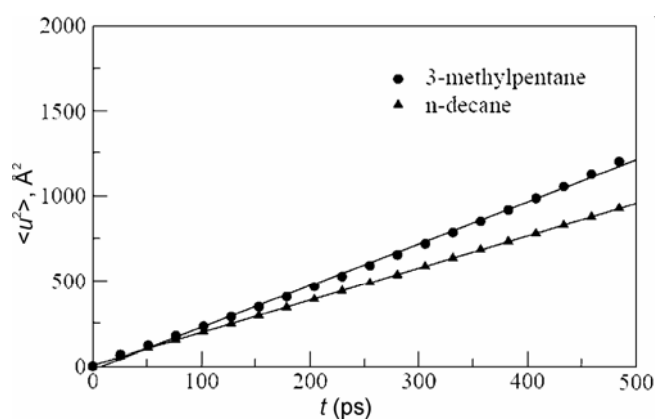


**Figure 4.** Mean square displacement of *n*-decane and 3-methylpentane at 300 K. Filled circles and triangles are the MD data for 3-methylpentane and *n*-decane respectively and the lines are least squares fit. The slope of 3-methylpentane is higher than *n*-decane and hence the diffusivity of 3-methylpentane is higher than *n*-decane.

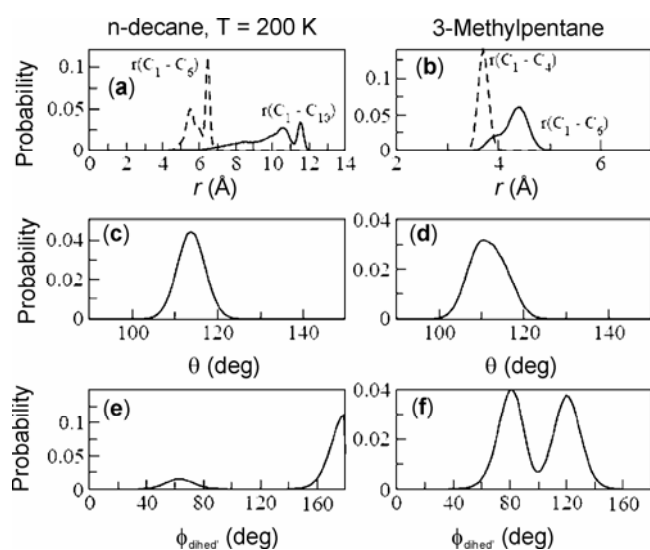


**Figure 3.** The top most panel (a) and (b) is the end–end distance distribution of the molecules, middle one (c) and (d) is the bond angle distribution and the lower most (e) and (f) panel is the dihedral angle distribution.

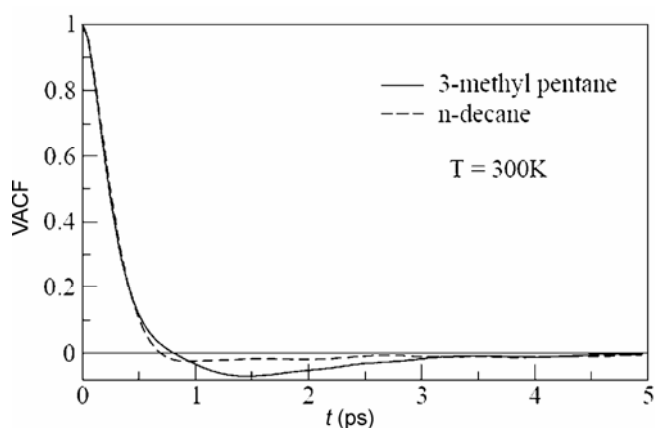


**Figure 5.** Velocity autocorrelation function of *n*-decane and 3-methylpentane at 300 K. 3-methylpentane has more back scattering than *n*-decane.

shown. The VACF of 3-methylpentane has more back scattering than *n*-decane. Previous studies have shown that in general the guest with higher self diffusivity will have lower back scattering.<sup>24</sup> In the present study this is not the case possibly because 3-methylpentane presumably does not always enter the 12-ring window with the long molecular axis perpendicular to this window plane. Due to molecular reorientations during diffusion, at times, it is expected that the molecular orientation differs from this orientation. When this is the case, the molecular cross-section will be smaller and as a consequence the levitation parameter will be less than 0.94. Under this situation, it is expected that the potential energy landscape associated with 3-methylpentane will have larger undulations leading to larger back scattering in the VACF. This might be responsible for the presence of significant back scattering. Physically, this means that the cross-section diameter of 3-methylpentane is still somewhat smaller in diameter than the 12-ring window.

The activation energy is calculated from Arrhenius plots. Figure 6 shows Arrhenius plots for *n*-decane and 3-methylpentane. From the slopes of the Arrhenius plots, the activation energy of 3-methylpentane is 3.7 kJ/mol which is less than 6.0 kJ/mol obtained for *n*-decane. This behaviour is in accordance with the previous predictions of levitation effect.

## 5. Conclusions

The present study suggests that the branched hydrocarbon 3-methylpentane has a higher self diffusivity

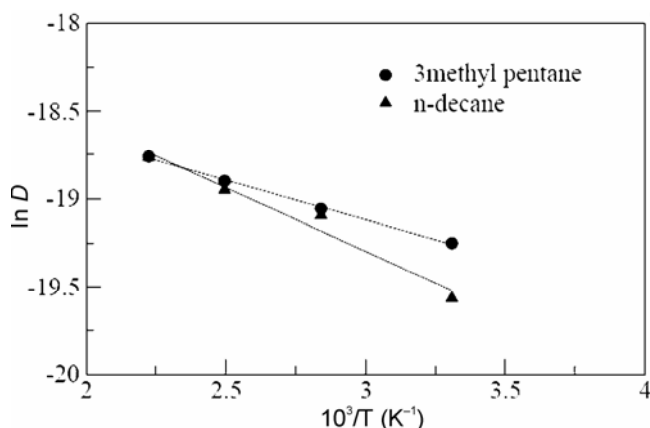


**Figure 6.** Arrhenius plot for *n*-decane and 3-methylpentane. The slope of 3-methylpentane is smaller than that of *n*-decane. The activation energy of 3-methylpentane is 3.7 kJ/mol and that of *n*-decane is 6.0 kJ/mol.

at room temperature as compared to *n*-decane in zeolite NaY. This behaviour is in agreement with the predictions of the levitation effect. Although the diameter of 3-methylpentane is somewhat smaller than the diameter of the 12-ring window, it is sufficiently large to exhibit many of the characteristics of the anomalous regime guest. One of the possible industrial applications of this is that branched hydrocarbons may be separated from linear hydrocarbons using the differences in their properties observed here. Typically, for such separations, a lower temperature would be preferred since diffusivities of the molecules to be separated are quite different at lower temperatures than at higher temperatures.

## Acknowledgements

Authors wish to thank the Department of Science and Technology, New Delhi. Council of Scientific and Industrial Research (CSIR), New Delhi, for financial support in carrying out this work as well as for Fellowship to BJB. This work makes use of results produced by the Cybersar Project managed by the Consorzio COSMOLAB, a project co-founded by the Italian Ministry of University and Research (MIUR) within the Programma Operativo Nazionale 2000–2006 ‘Ricerca Scientifica, Sviluppo Tecnologico, Alta Formazione’ per le Regioni Italiane dell’Obiettivo 1 (Campania, Calabria, Puglia, Basilicata, Sicilia, Sardegna) – Asse II, Misura II.2 ‘Società dell’Informazione’, Azione a ‘Sistemi di calcolo e simulazione ad alte prestazioni’. P D wish to thank the Consorzio Cosmolab for financial support to his Bangalore visit. S Y wishes to thank University of Sassari for a Visiting Professorship. F G P thanks Dipartimento di Chimica, Università di Sassari, Italy for granting leave of absence.

## References

1. Smit B and Maesen T L M 2008 *Chem. Rev.* **108** 4125
2. Smit B and Maesen T L M 1995 *Nature* **374** 42
3. Smit B and Maesen T L M 2008 *Nature* **451** 671
4. Vlugt T J H, Krishna R and Smit B 1999 *J. Phys. Chem.* **B103** 1102
5. Vlugt T J H, Zhu W, Kapteijn F, Moulijn J A, Smit B and Krishna R 1998 *J. Am. Chem. Soc.* **120** 5599
6. Chempath S, Krishna R and Snurr R Q 2004 *J. Phys. Chem.* **B108** 13481
7. Krishna R and van Baten J M 2006 *Chem. Phys. Lett.* **420** 545
8. Fox J P and Bates S P 2004 *J. Phys. Chem.* **B108** 17136

9. Liu H, Zhang Z, Chen B H and Zhao Y 2008 *J. Porous Mater* **15** 119
10. Lu L H, Wang Q and Liu Y C 2003 *Langmuir* **19** 10617
11. Webb E B, Grest G S and Mondello M 1999 *J. Phys. Chem.* **B103** 4949
12. Svelle S, Kolboe S and Swang O 2004 *J. Phys. Chem.* **B108** 2953
13. Yashonath S and Santikary P 1994 *J. Phys. Chem.* **98** 6368
14. Derouane E G 1987 *Chem. Phys. Lett.* **142** 200
15. Derycke I, Vigneron J P, Lambin P, Lucas A A and Derouane E G 1991 *J. Chem. Phys.* **94** 4620
16. Derouane E G, Andre J-M and Lucas A A 1988 *J. Catal.* **110** 58
17. Kemball C 1950 *Adv. Catal.* **2** 233
18. Jimenez-Cruz F and Laredo G C 2004 *Fuel* **83** 2189
19. Demontis P, Suffritti G B, Quartieri S, Fois E S and Gamba A 1988 *J. Phys. Chem.* **92** 867
20. Jorgensen W L, Madura J D and Swenson C J 1984 *J. Am. Chem. Soc.* **106** 6638
21. Nath S K and Khare R 2001 *J. Chem. Phys.* **115** 10837
22. Wender A, Barreau A, Lefebvre C, Di Lella A, Boutin A, Ungerer P and Fuchs A H 2007 *Adsorption* **13** 439
23. Smith W and Forester T R 2007 *DLPOLY-2.18 User manual*; CCLRC Daresbury Laboratory, Daresbury, UK
24. Bhide S Y and Yashonath S 2004 *Mol. Phys.* **102** 1057